Combining *M*- and *L*-edge resonant inelastic x-ray scattering for studies of 3*d* transition metal compounds

S. G. Chiuzbăian,[1,*] T. Schmitt,[2] M. Matsubara,[3] A. Kotani,[4,5] G. Ghiringhelli,[6] C. Dallera,[7] A. Tagliaferri,[8] L. Braicovich,[8] V. Scagnoli,[9] N. B. Brookes,[9] U. Staub,[2] and L. Patthey[2]

[1]*Laboratoire de Chimie Physique–Matière et Rayonnement, UPMC Université Paris 06, CNRS UMR 7614, 75005 Paris, France*

[2]*Swiss Light Source, Paul Scherrer Institut, CH-5232 Villigen PSI, Switzerland*

[3]*Laboratoire des Colloïdes, Verres et Nanomatèriaux (UMR 5587), Université Montpellier II, Place Eugène Bataillon, 34095 Montpellier Cedex 5, France*

[4]*RIKEN/Spring8, 1-1-1 Kouto, Sayo, Hyogo 679-5148, Japan*

[5]*Photon Factory, IMSS, High Energy Accelerator Research Organization, 1-1 Oho Tsukuba, Ibaragi 305-0801, Japan*

[6]*Dipartimento di Fisica, CNR/INFM Coherentia and SOFT, Politecnico di Milano, Piazza Leonardo da Vinci 32, 20133 Milano, Italy*

[7]*Dipartimento di Fisica, CNR/INFM ULTRAS, Politecnico di Milano, Piazza Leonardo da Vinci 32, 20133 Milano, Italy*

[8]*Dipartimento di Fisica, CNR/INFM SOFT, Politecnico di Milano, Piazza Leonardo da Vinci 32, 20133 Milano, Italy*

[9]*European Synchrotron Radiation Facility, BP 220, 38043 Grenoble Cedex, France*

(Received 15 July 2008; revised manuscript received 16 October 2008; published 2 December 2008)

Resonant inelastic x-ray scattering (RIXS) measurements performed jointly across the $M_{2,3}$ and L_3 absorption thresholds are used to study CoO local electronic structure and are supported by model calculations. The high-resolution experimental data provide a precise set of parameters to describe the correlated response of valence electrons. The *same* core-hole independent set of parameters within the single impurity Anderson model is used to describe *both* the *M* (3*p*-3*d*) and *L* (2*p*-3*d*) resonances. This work shows that combining *M* and *L* scattering data provides an enhanced contrast view of the spectral weights. Measured $M_{2,3}$-RIXS spectra are observed to be free of charge-transfer or normal fluorescence contributions. Moreover the cross section of *M*-RIXS final states with change in spin multiplicity is low. Combining this information with *L*-edge studies establishes an appealing means of making a better separation between on-site and intersite (ligand to metal) electronic excitations. Experimental and theoretical features specific to RIXS studies performed at *M* and *L* edges are summarized as a basis for future studies on complex transition metal compounds.

DOI: 10.1103/PhysRevB.78.245102 PACS number(s): 78.70.En, 71.70.Ch

I. INTRODUCTION

The investigation of electronic structure by means of resonant inelastic x-ray scattering (RIXS) has gained a privileged place in the mainstream of modern x-ray spectroscopic techniques.[1,2] Motivation for this type of approach arises from the insight that can be gained into the energetics of the electronic levels for strongly correlated materials especially as concerns intriguing properties such as superconductivity or colossal magnetoresistance. In RIXS experiments local excitations of valence electrons are revealed by means of photon scattering. The system is left either in the initial ground state (Rayleigh or elastic scattering) or in an excited state corresponding to local electronic excitations (inelastic scattering). The difference between the energy of incoming and outgoing photons displays the amount of energy transferred to the system and characterizes the excited final states. The topology of electronic excitations depends on the relative strength of on-site electron-electron interactions: for strong coupling the single-electron descriptions such as band structure approaches has to be replaced by the correlated response of electrons. It is important to observe that electric dipole transitions intervene twice in the RIXS process thus making it possible to examine unrestrictedly transitions between orbitals of same symmetry, in particular intraband *dd* or *ff* excitations. These correspond to neutral modifications of the *d*-level or *f*-level occupancy as a consequence of energy uptake. The specific energies of *dd* excitations deliver essential information on the crystal field acting on the metal site. Because they are dipole forbidden, they are accessible by other techniques such as optical-absorption spectroscopy only under limited conditions.

Since the demonstration that RIXS could explore *dd* excitations on the cation site in 3*d* transition metal (3*d* TM) compounds,[3] substantial progress has been made. For practical reasons relating to experimental accessibility, most studies with photon energies below 1000 eV aimed for $L_{2,3}$ edges. RIXS data at $M_{2,3}$ edges are relatively scarce[4–6] being hampered by very low count rates. The advances achieved in the last decade on the instrumental side illustrate that $L_{2,3}$-RIXS measurements with sub-eV combined energy resolution are nowadays readily available.[7,8] Recently it has also been shown that using high-flux and high-resolution beamlines in combination with suitable high-acceptance photon spectrometers, $M_{2,3}$-RIXS experiments are possible with good signal-to-noise ratios.[6] Theoretical frameworks accounting for on-site and intersite interactions have been developed with the modeling of experimental resonances delivering relevant information on the 3*d* valence electrons.[1,2] Having in mind the growing importance of studies on complex 3*d* TM compounds, it is timely to examine the complementarities between RIXS experiments performed at *L* and *M* thresholds.[9]

Here we present a joint experimental and theoretical RIXS study of local electronic excitations in CoO, an archetype for 3*d* TM compounds. The difficulties encountered in

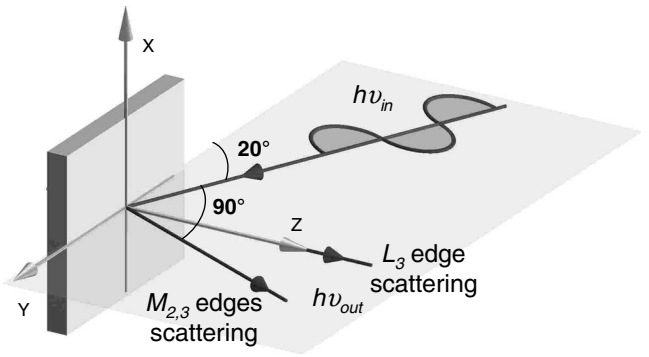

FIG. 1. Schematic view of the scattering geometry.

the theoretical description of ligand to metal electronic transfer at L-RIXS resonances[10,11] single out CoO as an ideal candidate for this study. Additionally the available knowledge base of theoretical and spectroscopic experimental findings on CoO allows us to draw technique-specific conclusions. We show Co $M_{2,3}$-RIXS experimental data as well as L_3-RIXS spectra recorded with improved energy resolution compared to the previous measurements.[11] The data were described with theoretical simulations performed within the single impurity Anderson model (SIAM). Core-hole independent parameters were chosen so as to be identical for both sets of spectra allowing for a coherent approach to RIXS and its capabilities in the soft x-ray region.

II. EXPERIMENTAL CONDITIONS AND RESULTS

The $M_{2,3}$-RIXS measurements were carried out at the "Surface/Interfaces Spectroscopy" beamline at the Swiss Light Source (Paul Scherrer Institut, Villigen, Switzerland). The base pressure in the vacuum chamber was better than 5×10^{-10} mbar. The beamline was operated with an exit slit opening of 200 μm resulting in a resolving power $E/\Delta E$ of approximately 3000 for the monochromator grating with 300 lines/mm grove density. Under these conditions the combined instrumental broadening is primarily due to the Rowland-mounting grazing incidence spectrometer[12] used for the detection of scattered photons. We used a 300 lines/mm spherical grating with a radius of 3 m and chose a 30 μm entrance slit. For the L_3-RIXS measurement we employed the advanced x-ray emission spectroscopy (AXES) spectrometer[13] installed at beamline ID08 of the European Synchrotron Radiation Facility (ESRF) in Grenoble, France. At this facility the beamline resolving power $E/\Delta E$ is better than 3000 using a 1400 lines/mm varied line spacing (VLS) grating of a dedicated monochromator. The spectrometer operates with a 2400 lines/mm holographic VLS grating.

All data acquisitions were performed at room temperature, above the antiferromagnetic ordering temperature $T_N \approx 288$ K. The sample was a single-crystal CoO(100) with the surface contained in a vertical plane (Fig. 1). At room temperature CoO features a rock-salt cubic structure, the Co ions with formal valence states 2+ (electronic configuration $3d^7$) being octahedrally surrounded by oxygen atoms. The incoming radiation was linearly polarized with the polarization vector contained in the horizontal scattering plane. For the $M_{2,3}$-edge measurements the scattered light was detected at 90° to the incident beam striking the sample at 20° grazing incidence. Same orientation of the sample against incoming beam was chosen for the L_3 experiments except that the scattering angle was 110°. The scattering angles are dictated by the fixed installed spectrometers.

The experimental $M_{2,3}$-RIXS data are summarized in Fig. 2. The measurements were performed for several incoming photon energies between 57.5 and 64.5 eV, sampling the

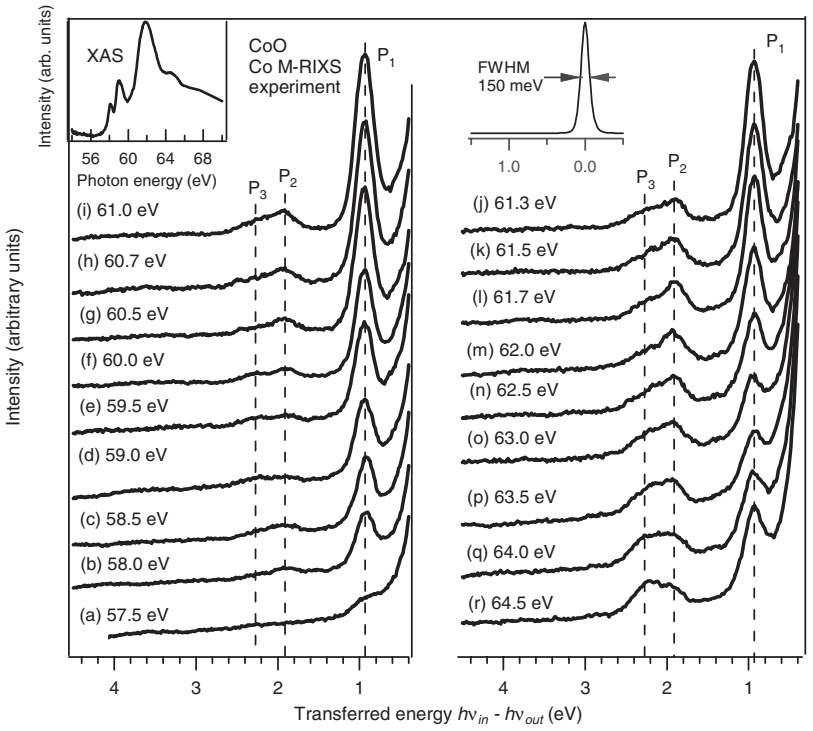

FIG. 2. RIXS spectra measured at the Co M threshold in CoO. Vertical dashed lines are a guide to help identify the spectral features (see text for further information). All spectra are normalized to the acquisition time and incoming photon flux, the average recording time per spectrum being about 2 h. The abscissa represents the difference between the energies of incoming and scattered photons $h\nu_{in}-h\nu_{out}$. The left inset reproduces the shape of the Co $M_{2,3}$ absorption spectra deduced from reflectivity measurements (Ref. 14). The right inset shows the shape of the spectrum measured for 57.5 eV incoming x rays and displays the FWHM of the elastic peak.

Co *M* absorption edge, itself derived from reflectivity measurements.[14] We note that we attempted to record the *M*-edge absorption curve with a standard setup featuring screened cables, inside and outside vacuum, and a picoampmeter. Due to the weakness of the *M* resonances, it was not possible to distinguish a usable absorption spectrum from the background when scanning the energy from 50 to 70 eV. The combined energy resolution of *M*-RIXS measurements was about 150 meV as indicated by the full width at half maximum (FWHM) of the elastic peak (see inset of Fig. 2). The dispersion on the detector corresponds to approximately 55 channels/eV. This made it possible to follow three well-resolved inelastic peaks (P_1, P_2, and P_3) situated within the first 2.5 eV transferred energy. The spectra are dominated by the contribution of elastically scattered photons, typically having an intensity larger by about 2–3 orders of magnitude and therefore truncated in Fig. 2. As previously observed for NiO, all measured spectral features follow a remarkable Raman behavior.[6] Among the losses, the intensity of P_1 centered at 0.93 eV is dominant at all incoming photon energies, reaching a maximum amplitude at 61.0 eV excitation. An important output of these measurements is the clear 0.4 eV separation between P_2 and P_3, which was not resolved up to now by other techniques.[15–19] Both P_2 and P_3 are already distinguishable for 60.0 eV incoming photons and become sizable for excitations higher than 63 eV. At 64.0 eV there is a change in the relative weight of P_2 and P_3.

Figure 3 shows the measured L_3-RIXS curves detected with a combined energy resolution of 0.5 eV. The sampling step was 55 meV but for clarity the data points are not explicitly represented. Compared to the previous *L*-RIXS measurements[11] on CoO, an effective resolving power gain is visible. The elastic peak P_0 is well separated from the first loss structure P_1 for all excitations, an extra feature P_4 is resolved for excitation B and appears as a shoulder for incoming x-rays with energy C. We denote the second visible peak as $P_{2,3}$ for consistency with the notation of Fig. 2. This is possible since the final states measured in both scattering experiments are the same irrespective of the investigated resonance. Dashed lines indicate the positions of P_2 and P_3 as measured by $M_{2,3}$-RIXS. A broad band of weak excitations dispersing on a transferred energy scale is visible between 4 and 12 eV and can be attributed to ligand to metal charge-transfer (CT) transitions.[11] The states within 3 eV of the elastic peak feature dominant Raman behavior and are due to intraband *dd* excitations, as underlined below.

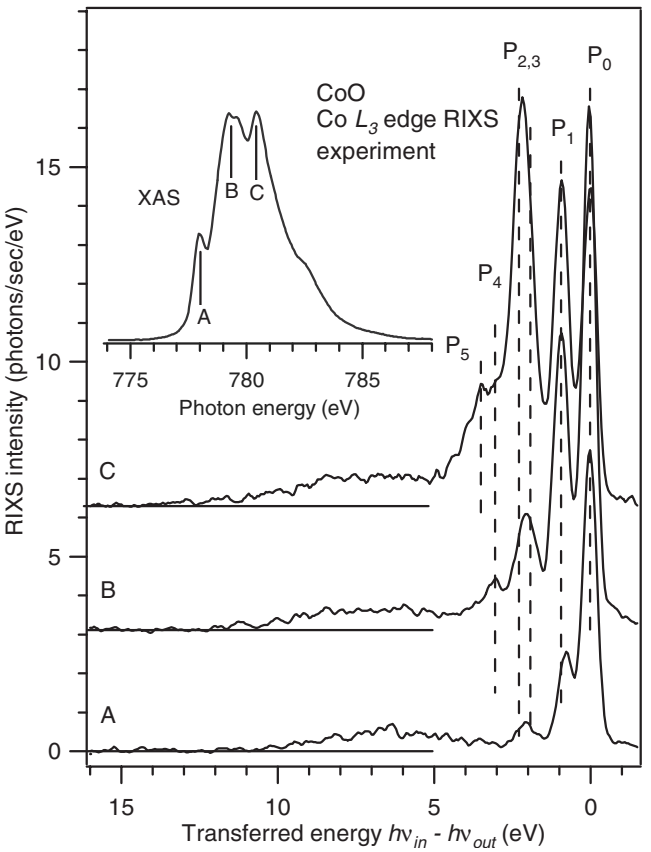

FIG. 3. Representative L_3-RIXS experimental data set along with the corresponding x-ray absorption curve detected in total electron yield mode (inset). The excitations energies used for scattering measurements are indicated with vertical bars. The notation of observed losses (vertical dashed lines) was made in compliance with the one used in Fig. 2 (see text also).

III. COMPUTATIONAL METHOD AND SPECTRA SIMULATIONS

For assessing the nature of measured resonances beyond the simple ionic picture, we considered a $(CoO_6)^{10-}$ cluster described within the SIAM, as previously implemented with success.[20] Within this framework the Co $3d$ valence electrons mix with O $2p$ states, the latter being modeled as equally spaced states within a finite width energy band *W*. In a simplified view the mixture between $3d^7$ and $3d^8\underline{L}$ configurations ($\underline{L}$ indicates an O $2p$ hole) displays an electronic structure generally consisting of a nonbonding band spanned by discrete bonding and antibonding states. This picture is altered by the inclusion of multiplet splittings of each configuration. The metal-ligand interaction is taken into account by the hybridization strengths $V(e_g)=-2V(t_{2g})$. Rescaling factors R_c and $1/R_v$ of hybridization strengths are incorporated to take into consideration the perturbations of $3d$ wave functions induced by the creation of a core hole ($R_c \leq 1$, i.e., contraction) or by ligand to metal charge transfer ($1/R_v > 1$, i.e., extension). Spin-orbit coupling constants, $\xi(3d)$ and $\xi(np)$, were included from an atomic Hartree-Fock calculation. The same source was used as input for the Slater integrals, F^k and G^k, entering the atomic term of the Hamiltonian, but these were scaled down to 80% prior to inclusion into the SIAM cluster model. The RIXS cross sections were calculated using the Kramers-Heisenberg formula at 0 K, considering the same geometry in respect to the x-ray polarization as in the experiments. The intermediate-state broadening was taken as 0.4 eV in the L_3 region[21] and 1.6 eV at the $M_{2,3}$ resonances.[22] Considering the width of the oxygen ligand band, $W=4.0$ eV, the parameters used to ensure best agreement with both sets of theoretical data are charge-transfer energy $\Delta=3.0$ eV, on-site *dd* Coulomb interaction $U_{dd}=6.8$ eV, hybridization energies $V(e_g)=2.1$ eV with rescaling factors, $R_c=0.8$ and $R_v=0.9$, crystal-field splitting en-

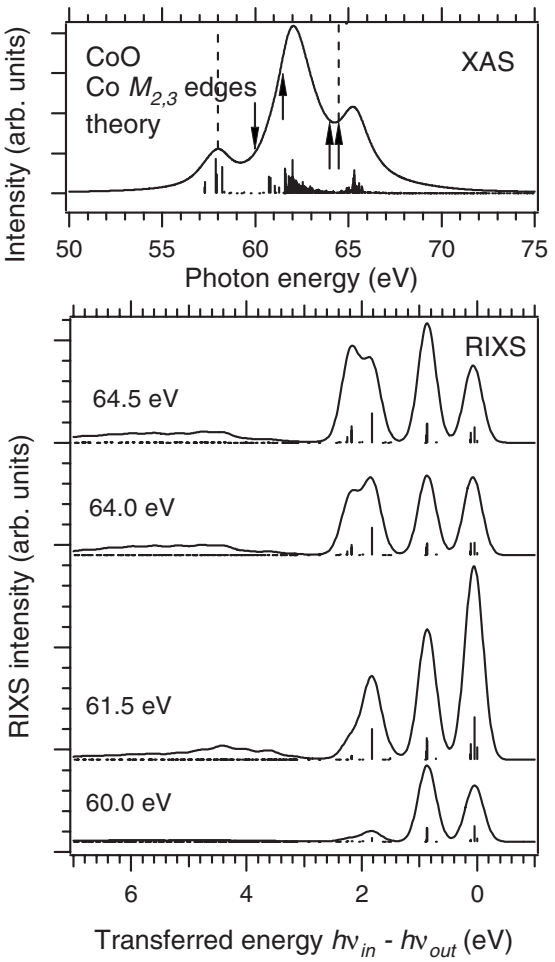

FIG. 4. Calculated x-ray absorption cross section (top) and RIXS intensities for four selected incoming photon energies (bottom).

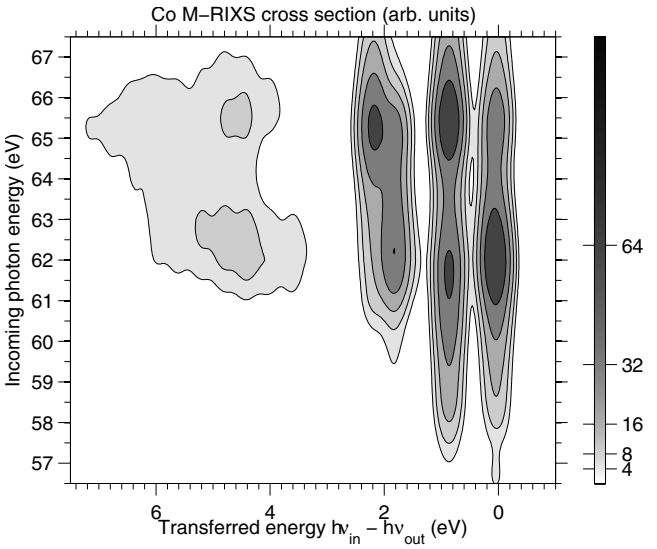

FIG. 5. Computational results for the RIXS cross section for *M* resonances of Co in CoO. The levels of the contour plot (identical with the ticks of lateral color bar) are chosen in order to emphasize the states below −3 eV relative energy. The map was generated by incrementing the incoming photon energy with 0.5 eV steps and convoluting each spectrum with 0.15 eV FWHM Gaussian to account for experimental broadening. Points along constant transferred energy lines were generated by spline interpolation.

ergy $10Dq=0.4$ eV (see Ref. 20 for a detailed description of all parameters). The O $2p$ band width affects the width of charge-transfer structure in RIXS spectra, as previously exemplified[20] for the case of NiO. The core hole related parameters reflect the different interaction strengths with valence electrons (core-hole potentials), the present simulations using $U_{dc}(2p)=8.0$ eV and $U_{dc}(3p)=7.6$ eV.

The main results of our spectra simulations are displayed in Figs. 4–6, a consistent agreement with the experiment being achieved, within the limits of the model. In particular the *M*-RIXS simulations provide a good description not only of the positions but also of the intensity dependence of all measured peaks. Vertical sticks in Figs. 4 and 6 display the energies and relative transition probabilities for all possible multiplet terms for both absorption case (electric dipole transitions to core-hole final states) and resonant scattering case (calculated according to the Kramers-Heisenberg relation). The agreement between experimental findings and theoretical predictions is discussed in detail in Sec. IV.

IV. DATA ANALYSIS

Striking differences between *M*- and *L*-RIXS experiments arise from the relative intensity of elastic peaks P_0. This observation is essentially material independent[6,23] and well exemplified by the present results: for the *M*-RIXS data the ratio between the intensity of the elastic peak and losses is roughly 500 for 61.0 eV excitation energy. On the other hand *L*-RIXS data feature comparable intensities for both elastic and inelastic channels. We recall that in the soft x-ray region most RIXS experiments are performed in 90° scattering geometry, i.e., the angle between the wave vectors of incoming and scattered light. Such a setup minimizes elastic scattering from the target for linearly polarized incoming photons in the scattering plane since the Brewster angle in the soft x-ray range is close to 45°. When moving toward the extreme ultraviolet energy range, the Brewster angle displays significant deviation from 45°. An intense elastic peak for *M*-RIXS measurements at 90° scattering geometry is observed and predictable[24] due to the huge increase in diffuse reflected light at slightly off-Brewster conditions.[25] It also explains the imbalance relative to theoretically predicted recombination transition probabilities. For *L*-RIXS even for 110° scattering angle the elastically scattered photon channel is quite weak and is less susceptible to mask inelastic events. Moreover the spectra simulations indicate that the spectral weight measured in the elastic channel is little or not at all influenced by the diffuse surface reflectivity. This explains the enhanced versatility of *L*-RIXS especially in the case of geometry-dependent RIXS measurements,[9] as well as for other purposes, such as choosing a geometry to minimize self-absorption effects. The consequences of the presence of the elastic peak can be easily overlooked for *M*-RIXS approaches. In particular serious difficulties with detector saturation problems due to intense diffuse light are encountered when performing *M*-RIXS measurements. Minimizing the

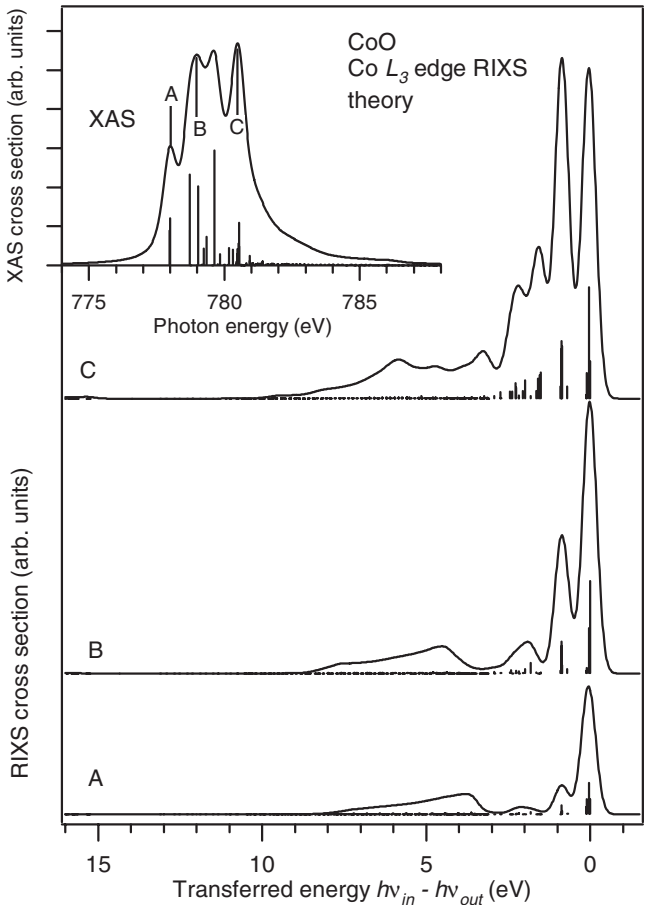

FIG. 6. Results of theoretical simulations performed for L_3-RIXS case. The inset displays the corresponding absorption edge.

weight of diffuse light by adapting scattering geometry in *M*-RIXS experiments is a challenging task. This would require, in the first place, the possibility to vary experimentally the scattering angle with subdegree precision. Even so, deviations of few degrees from the optimum scattering angle would result in a substantial increase in diffused light. This is in contradiction to the need for large angular acceptance spectrometers to overcome the very low *M*-RIXS cross section. We note that the spectrometer used in this work for *M*-RIXS measurements features an angular acceptance of about 5° in the scattering plane.

Turning now to the analysis of the inelastic part, it can be observed that the SIAM model reproduces well position and intensities of *L*-RIXS structures, especially for A and B excitations. In the case of incoming light with energy C the intensity of $P_{2,3}$ is underestimated, while the calculated result by Magnuson *et al.*[11] gives better agreement with the experimental one. The most striking difference between the calculation by Magnuson *et al.*[11] and ours is the existence of the (superexchange) exchange interactions which correspond to strong effective magnetic field. Magnuson *et al.*[11] took the exchange interactions into account while we did not. By inclusion of the exchange interactions, the spectral shapes are more or less modified. As a result, the calculated result of *L*-RIXS at energy C by Magnuson *et al.*[11] is in better agreement with the experimental result than our calculated result. However, inclusion of the exchange interactions also affects the spectral shape of x-ray absorption spectra (XAS) and the calculated result of *L*-edge XAS by Magnuson *et al.*[11] fails to reproduce the experimental result. Most notably, the spectral shape around energy B shows a clear two peak structure both in the experimental and our calculated results, while it is single peak structure in the calculated result by Magnuson *et al.*[11] Considering the fact that *L* XAS final state is the intermediate state of *L*-RIXS, it is inevitable to reproduce *L* XAS as precisely as possible in order to describe *L*-RIXS spectra reasonably. This is the main reason why we do not include the exchange interactions in our calculation. Thus, the underestimation of the intensity of $P_{2,3}$ at energy C remains to be solved here as a future problem as well as the quantitative analysis of the effect of the exchange interactions on the spectral shapes.

Typically three intrinsically different contributions are expected to interfere:[1] crystal-field *dd* excitations, CT contributions due to electron transfer from ligand to metal site ($3d^8\underline{L}$), and normal emission lines (fluorescence). The last term denotes excitation energy-independent spectral weight. Tracing back the weight of fluorescence lines on top of dispersive losses is eased by higher-resolution measurements. However, the fluorescence signal is expected to play only a minor role in the L_3 region. It is not included in the theoretical framework employed here. The emergence of *dd* excitations in RIXS spectra leads to Raman-type features.[3] In accordance with classical Raman spectroscopy, the label denotes losses which show up at constant transferred energy $\Delta\varepsilon = h\nu_{\mathrm{in}} - h\nu_{\mathrm{out}}$; i.e., they disperse with the incoming photon energy. We note, however, that the measured spectra represent envelopes of contributions resulting from branching of spectroscopic atomic terms in the crystal field. Obviously if two features are close to each other, the barycenter of their envelope may shift upon resonant excitation. This is exemplified by P_1 and excitation A at L_3 edge. As expected from previous studies[11] and confirmed by the simulations presented, the structures P_1 and $P_{2,3}$ display the energies needed for the lowest possible *dd* excitations.

In order to determine the incident photon energies for the *M*-RIXS calculation, we use constant-initial-state (CIS) data taken by resonant photoemission experiment by Shen *et al.*[26] as a reference because directly measured XAS data of *M* edge is not available. Since CIS data consist of the intensity of photoemission as a function of photon energies, the structures in CIS curves correspond to those of XAS. *M*-RIXS measurements display a remarkably good agreement so that the energy of lowest-lying crystal-field excitations can unambiguously be assigned to 0.93, 1.90, and 2.30 eV. In *M*-RIXS measurements the intensity of P_2 is larger than that of P_3 up to 64.0 eV incoming x-ray energies, but at 64.5 eV the P_3 intensity becomes larger than P_2 intensity (see Fig. 2). This reversal behavior of intensity ratio between P_2 and P_3 is successfully reproduced by our calculation. This important experimental achievement should stimulate further efforts on crystal-field *ab initio* calculations as the numerical convergence is still modest. As far as the replication of crystal-field energies in SIAM is concerned, *dd* energies are essentially described by the reduced Slater integrals (F^k, G^k), hybridiza-

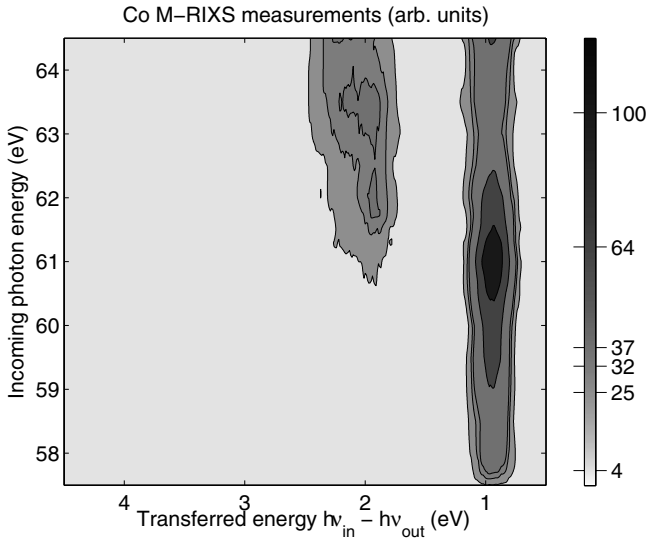

FIG. 7. Experimental results obtained at the Co *M* resonances in CoO presented as a two-dimensional map. We considered the spectra from Fig. 2 and subtracted the background fitting the tail of the elastic peak. The points along constant transfer energy lines were calculated by spline interpolation.

tion energies $[V(e_g), V(t_{2g})]$ and crystal-field splitting $10Dq$. We recall that the current $10Dq$ value should not be taken in classical sense of optical spectroscopy;[7,17] it merely represents the energy separation between e_g and t_{2g} Co $3d$ levels in an octahedral O_h crystal field in absence of Co-O hybridization. While our parameters are in good agreement with previous evaluations, they effectively rely on the reproduction of *M*- and *L*-RIXS spectral weights. This is a key aspect of our study: as RIXS measures core-hole free excited states, the combination of both *M*- and *L*-RIXS edges sets very strong boundary conditions for the choice of numerical parameters.

Current experimental and theoretical data also confirm that all visible *M*-RIXS spectra (Fig. 7) are due to crystal-field *dd* excitations only. To this end we considered appropriate charge-transfer energy Δ, width of the oxygen ligand band *W*, and hybridization energy, such that the broad band associated to CT excitations (higher than about 3 eV in *L*-RIXS spectra) is well described. As these parameters are core-hole independent they should also deliver a reliable estimation of CT spectral weights in *M*-RIXS spectra within the limits of our model. The contour plot of Fig. 5 depicts the magnitude of expected CT features at relative energies higher than 3.4 eV. We find that the corresponding CT band is below the detection limit of our experiment, an aspect which should be addressed in future instrumental developments. We add that our theoretical predictions for CT intensities in the *M*-RIXS spectra were rendered possible by the joint *M*- and *L*-RIXS study. The weakness of CT features in *M*-RIXS is probably related to the lower $3p$ core-hole potential: in *L*-RIXS studies the local perturbation applied to valence electrons is stronger. As a consequence the probability for ligand electrons to move onto the metal site and screen the core-hole is increased, finally leading to higher participation of scattering channels toward final states with CT. Our statement is based on two sets of *M*-RIXS data only, namely, the actual CoO measurements and the NiO results.[6] It would need to be backed up by further detailed studies on the late $3d$ TM compounds.

This observation sheds light on the observable CT structures in *L*-RIXS spectra. While being genuine Raman transitions, CT peaks present mixed behavior as they look similar to fluorescence within the O $2p$ bandwidth.[20] For this reason the experimental contrast still involves uncertainties despite advances in high-resolution detection of scattered photons over the last decade. Exceptions exist for convenient interplay of electronic parameters. For instance in the case of manganese and nickel $L_{2,3}$ spectra of simple monoxides, the associated *dd* contribution can be essentially interpreted in a simple crystal-field multiplet picture.[7,23] In both cases the CT spectral weight is well separated from the most intense crystal-field *dd* signatures. For this reason CoO turns up to be an appropriate test material as the overlap between *dd* excitation band and charge-transfer bands is effective[10] between 3 and 5 eV on a transferred energy scale. This spectral region is still a matter of debate with respect to characteristic *dd* energies;[11] it is not accessible with optical spectroscopies[15,17,19] or electron-energy-loss spectroscopy,[16,18] the multiplet energies extracted in crystal-field calculations being still scattered over larger intervals.[27,28] The crystal-field multiplets expected in this energy region would be mainly derived from atomic states with spin multiplicity 2 (doublets). In contrast those below 3 eV transferred energy arise from atomic spectral terms with spin multiplicity 4 (quartets), as in the ground state. In *M*-RIXS measured and simulated spectra the region situated between 3 and 5 eV displays no signatures of crystal-field *dd* excitations. This is an indication that in the octahedral symmetry the lower $3p$ spin-orbit coupling might be insufficient to allow *dd* transitions involving the flip of a single-electron spin (change in spin multiplicity). The *L*-RIXS spectra are richer in features between 3 and 5 eV transferred energy, and they show the presence of doublet final states. Nevertheless assessing the precise origin of P_4 and P_5 remains complicated. In the calculations the inclusion of hybridization attenuates the *L*-RIXS intensities expected from doublet final states, as derived in simpler crystal-field simulations. The sizeable differences between scattering channels to final states with different spin multiplicity and/or with charge transfer in *M* and *L*-RIXS are also expected to complement the information arising from studies of CT spectral weight performed at $3d$ TM *K* edges, as for instance on NiO (Ref. 29) and CoO (Ref. 30).

V. *L* AND *M*-RIXS

Bearing in mind future studies on $3d$ TM compounds it appears useful to review the main issues characterizing RIXS measurements at both edges of late $3d$ TM's compounds. Certain aspects (i)–(vii) are already known but briefly reviewed here for the sake of clarity.

(i) The initial (ground) states are identical irrespective of the intermediate resonantly excited core-hole state.

(ii) Final-state energies are also the same, irrespective of the excitation resonance. In both *L* and *M*-RIXS varying the

energy of incoming x rays has strong impact on the spectra of scattered photons but the transition rates to possible final states are different, a consequence of the fact that different choices for the participation of intermediate core-hole states are made. The following two aspects are relevant in this respect.

(iii) The spin-obit interaction is roughly 1 order of magnitude larger for excited $2p$ core-hole states in $3d$ TM compounds (3.77–13.50 eV) as compared to the $3p$ core holes (0.43–1.62 eV).[31,32]

(iv) The lifetime of $2p$ core holes is approximately ten times larger when compared to $3p$ core holes,[33] resulting in a corresponding reduced broadening of the intermediate states' spectral distribution.

These are illustrated for instance by the x-ray absorption measurements performed across the *M* and *L* edges of simple nickel compounds.[34,35] Two further points can be directly derived.

(v) The selectivity for scattering channels is coarser in *M*-RIXS experiments, practically both spin-orbit branches being always involved in the scattering process. For *L*-RIXS the L_3 channel is easily separable.

(vi) The time scale accessible in core-hole clock experiments[36] should be different depending on the excited core-hole state.

Significant differences between the two approaches arise from the particular bulk sensitivities and reflectivity properties.

(vii) The attenuation length for x rays covering *L* edges of $3d$ TM is on the order of hundreds of nanometer compared to tens of nanometer for *M* edges.[25] In consequence the latter has a relatively higher surface sensitivity, especially relevant for small grazing incidence geometries.

The reflectivity can vary by as much as 4 orders of magnitude between the *M*- (high-reflectivity) and the *L*-edges (low-reflectivity) regions.[25] This leads to typically large diffuse scattering from surface imperfections below 100 eV.[24] The outcome is the presence of a very strong peak matching the energy of incoming photons, which poses serious limitations. Last but not least it restricts attainable incoming polarization dependence studies, incoming light with out-of-scattering plane components being particularly concerned.

On the experimental side the extremely low cross section of the *M*-RIXS process results in low counting rates at the detector. Nevertheless *M*-RIXS measurements provide a good "absolute energy resolution to counting rate" ratio. In other words measuring *L*-RIXS spectra with comparable resolution leads inescapably to the use of spectrometers with lower throughput which partially takes away the cross-section advantage.

Three seminal aspects are derived from the data presented here.

(i) In the case of *M*-edge spectra the contribution from fluorescence decay is below the detection limit over the whole energy range.

(ii) *M*-edge spectra are expected to feature a pure Raman character directly delivering information relevant to local neutral excitations.

(iii) Final states arising from charge-transfer excitations are presumably very weak and not detectable for excitations across the $M_{2,3}$ resonances.

VI. CONCLUSIONS

We described high-resolution L_3- and $M_{2,3}$-RIXS data taken on CoO within a consistent theoretical model. We conclude all measured *M*-RIXS resonances are due to *dd* excitations, this enables a much clearer view on the energetic overlap of crystal-field and charge-transfer excitations at the L_3 edge. Strong constraints imposed on the theoretical approach by both sets of data mean that a very reliable set of parameters to describe the local electronic structure of CoO are obtained. On this basis we discuss the spectral contrast achievable in the charge-transfer region as well as for RIXS final states with change in spin multiplicity.

ACKNOWLEDGMENTS

The *M*-RIXS measurements were performed at the Swiss Light Source, Paul Scherrer Institut, Villigen, Switzerland. The L_3-RIXS data were taken at the ESRF using the AXES instrumentation within the AXES contract, between the ESRF and the INFM/CNR. We would like to thank T. Uozumi for providing us with his computer program used in our RIXS calculations. S.G.C. is deeply indebted to Coryn F. Hague for stimulating discussions.

*gheorghe.chiuzbaian@upmc.fr

[1] A. Kotani and S. Shin, Rev. Mod. Phys. **73**, 203 (2001).
[2] A. Kotani, Eur. Phys. J. B **47**, 3 (2005).
[3] S. M. Butorin, J.-H. Guo, M. Magnuson, P. Kuiper, and J. Nordgren, Phys. Rev. B **54**, 4405 (1996).
[4] P. Kuiper, J. H. Guo, C. Såthe, L. C. Duda, J. Nordgren, J. J. M. Pothuizen, F. M. F. de Groot, and G. A. Sawatzky, Phys. Rev. Lett. **80**, 5204 (1998).
[5] L.-C. Duda, T. Schmitt, J. Nordgren, G. Dhalenne, and A. Revcolevschi, Surf. Rev. Lett. **9**, 1103 (2002).
[6] S. G. Chiuzbăian, G. Ghiringhelli, C. Dallera, M. Grioni, P. Amann, X. Wang, L. Braicovich, and L. Patthey, Phys. Rev. Lett. **95**, 197402 (2005).
[7] G. Ghiringhelli, M. Matsubara, C. Dallera, F. Fracassi, A. Tagliaferri, N. B. Brookes, A. Kotani, and L. Braicovich, Phys. Rev. B **73**, 035111 (2006).
[8] C. F. Hague, J.-M. Mariot, V. Ilakovac, R. Delaunay, M. Marsi, M. Sacchi, J.-P. Rueff, and W. Felsch, Phys. Rev. B **77**, 045132 (2008).
[9] M. van Veenendaal, Phys. Rev. Lett. **96**, 117404 (2006).
[10] S. M. Butorin, J. Electron Spectrosc. Relat. Phenom. **110-111**, 213 (2000).
[11] M. Magnuson, S. M. Butorin, J.-H. Guo, and J. Nordgren, Phys. Rev. B **65**, 205106 (2002).
[12] J. Nordgren and R. Nyholm, Nucl. Instrum. Methods Phys. Res. A **246**, 242 (1986).

[13] C. Dallera, E. Puppin, A. Fasana, G. Trezzi, N. Incorvaia, L. Braicovich, N. B. Brookes, and J. B. Goedkoop, J. Synchrotron Radiat. **3**, 231 (1996).
[14] R. Berlasso, C. Dallera, F. Borgatti, C. Vozzi, G. Sansone, S. Stagira, M. Nisoli, G. Ghiringhelli, P. Villoresi, L. Poletto, M. Pascolini, S. Nannarone, S. De Silvestri, and L. Braicovich, Phys. Rev. B **73**, 115101 (2006).
[15] G. W. Pratt and R. Coelho, Phys. Rev. **116**, 281 (1959).
[16] A. Gorschlüter and H. Merz, Phys. Rev. B **49**, 17293 (1994).
[17] M. Haβel, H. Kuhlenbeck, H.-J. Freund, S. Shi, A. Freitag, V. Staemmler, S. Lütkehoff, and M. Neumann, Chem. Phys. Lett. **240**, 205 (1995).
[18] B. Fromme, M. Möller, C. Bethke, U. Brunokowski, and E. Kisker, Phys. Rev. B **57**, 12069 (1998).
[19] M. Fiebig, T. Lottermoser, V. V. Pavlov, and R. V. Pisarev, J. Appl. Phys. **93**, 6900 (2003).
[20] M. Matsubara, T. Uozumi, A. Kotani, and J.-C. Parlebas, J. Phys. Soc. Jpn. **74**, 2052 (2005).
[21] M. O. Krause and J. H. Oliver, J. Phys. Chem. Ref. Data **8**, 329 (1979).
[22] L. I. Yin, I. Adler, T. Tsang, M. H. Chen, D. A. Ringers, and B. Crasemann, Phys. Rev. A **9**, 1070 (1974).
[23] G. Ghiringhelli, M. Matsubara, C. Dallera, F. Fracassi, R. Gusmeroli, A. Piazzalunga, A. Tagliaferri, N. B. Brookes, A. Kotani, and L. Braicovich, J. Phys.: Condens. Matter **17**, 5397 (2005).
[24] D. L. Windt, Comput. Phys. **12**, 360 (1998).
[25] See center for x-ray optics database, url http://www.cxro.msd.lbl.gov/
[26] Z.-X. Shen, J. W. Allen, P. A. P. Lindberg, D. S. Dessau, B. O. Wells, A. Borg, W. Ellis, J. S. Kang, S.-J. Oh, I. Lindau, and W. E. Spicer, Phys. Rev. B **42**, 1817 (1990).
[27] C. de Graaf, W. A. de Jong, R. Broer, and W. C. Nieuwpoort, Chem. Phys. **237**, 59 (1998).
[28] O. Ney, M. Trzeciecki, and W. Hübner, J. Phys.: Condens. Matter **17**, 7489 (2005).
[29] A. Shukla, J.-P. Rueff, J. Badro, G. Vanko, A. Mattila, F. M. F. de Groot, and F. Sette, Phys. Rev. B **67**, 081101(R) (2003).
[30] J.-P. Rueff (private communication).
[31] G. van der Laan, J. Phys.: Condens. Matter **3**, 7443 (1991).
[32] G. van der Laan and I. W. Kirkman, J. Phys.: Condens. Matter **4**, 4189 (1992).
[33] O. Keski-Rahkonen and M. O. Krause, At. Data Nucl. Data Tables **14**, 139 (1974).
[34] S. Nakai, H. Nakamori, A. Tomota, H. Nakamura, and C. Sugiura, Phys. Rev. B **9**, 1870 (1974).
[35] G. van der Laan, J. Zaanen, G. A. Sawatzky, R. Karnatak, and J.-M. Esteva, Phys. Rev. B **33**, 4253 (1986).
[36] L. Braicovich, G. Ghiringhelli, A. Tagliaferri, G. van der Laan, E. Annese, and N. B. Brookes, Phys. Rev. Lett. **95**, 267402 (2005).